Int J Thermophys (2010) 31:150–162
DOI 10.1007/s10765-009-0659-2

Analysis of Possibilities of Application of Nanofabricated Thermal Probes to Quantitative Thermal Measurements

Jerzy Bodzenta · Anna Kaźmierczak-Bałata · Maciej Lorenc · Justyna Juszczyk

Received: 15 April 2009 / Accepted: 28 September 2009 / Published online: 20 October 2009
© Springer Science+Business Media, LLC 2009

Abstract A steady-state thermal model of the nanofabricated thermal probe was proposed. The resistive type probe working in the active mode was considered. The model is based on finite element analysis of the temperature field in the probe-sample system. Determination of the temperature distribution in this system allows calculations of relative changes in the probe electrical resistance. It is shown that the modeled probe can be used for measurements of the local thermal conductivity with the spatial resolution determined by the probe apex dimensions. The probe exhibits the maximum sensitivity to the changes in the thermal conductivity of the sample between $2\ \mathrm{W \cdot m^{-1} \cdot K^{-1}}$ and $200\ \mathrm{W \cdot m^{-1} \cdot K^{-1}}$. The influence of the thermal conductivity of the probe substrate on metrological characteristics of the probe as well as the thermal resistance of the probe-sample contact on the determination of the sample thermal conductivity were also analyzed. The selected results of numerical analysis were compared with data of preliminary experiments.

Keywords Finite element analysis · Nanofabricated thermal probe · Scanning thermal microscopy · Thermal conductivity · Thermal measurement

1 Introduction

The development of materials science and technology results in widespread application of sophisticated material structures. Very often components of these structures have dimensions smaller than 1 μm and in the case of so called nanostructures—dimensions smaller than 100 nm. Thin films are the most popular submicron structures. They are used as passive and active elements in electronic devices, protective coatings,

J. Bodzenta (✉) · A. Kaźmierczak-Bałata · M. Lorenc · J. Juszczyk
Institute of Physics, Silesian University of Technology, Krzywoustego 2, 44-100 Gliwice, Poland
e-mail: Jerzy.Bodzenta@polsl.pl

antireflective coatings, etc. In many applications, the thermal properties of thin films play a key role. They are clearly seen in the area of electronic and photonic devices. The growing scale of integration and operation at high frequencies and high powers lead to the appearance of high-density heat sources in the devices. Thus, the effective heat abstraction becomes critical to device performance (see, e.g., [1,2]). To solve this problem, new materials are investigated [3,4] and new cooling techniques are proposed [5].

The design of effective cooling systems at the submicron scale is additionally complicated because of difficulties with prediction of the thermal conductivity of thin films [6]. Structural defects and thermal resistances at boundaries cause that the thermal conductivity of thin dielectric films is considerably lower than that of the respective bulk materials. Separate problems involve understanding and modeling of the heat transport in nanostructures. New effects connected with transport phenomena in such structures are intensively studied (e.g., [7–10]). However, first of all, the investigation of thermal properties of submicron structures requires methods of experimental determination of these properties.

Parameters describing the heat transport in solids are the thermal conductivity, κ, and the thermal diffusivity, α. They are related through the volumetric heat capacity C,

$$\kappa = \alpha C. \tag{1}$$

Standard measuring techniques used for determination of these parameters cannot be applied to investigation of submicron structures. This is why new experimental techniques were developed. A comprehensive review of these methods can be found in Ref. [1]. They are also briefly summarized in Ref. [6].

One of the most promising methods allowing the investigation of thermal properties with high spatial resolution is scanning thermal microscopy (SThM). In 1986 Williams and Wickramasinghe [11] proposed modification of a structure of a just developed atomic force microscope (AFM) [12]. The modification consisted of replacement of a cantilever, for which the tip interacts with a sample by van der Waals forces, by the cantilever with a thermocouple at the tip. The tip was heated with an electric current. Topography of the sample surface was determined by ensuring constant temperature of the tip. This required a constant tip–sample distance. The device, called a scanning thermal profiler, allowed noncontact profiling. The same device was also used as a high resolution thermal microscope [13]. It was the beginning of SThM. Nowadays, the SThM measurements are typically performed by the use of AFM equipped with a special thermal module. The most common thermal probes (ThPs) used in SThM are resistance sensors. The device can operate in the passive and active modes. In the passive mode, the ThP measures the local temperature of the sample. In the active mode the ThP serves also as a heater. The signal from the ThP depends on the efficiency of the heat abstraction from the probe to the sample. Consequently, imaging of regions with different thermal conductivities is possible. A detailed description of the SThM technique at different stages of its development can be found in review papers [14–16].

SThM images obtained in the active mode give qualitative information about the thermal properties of the sample. A question raises if it is possible to obtain quantitative

characterization of the heat transport in the sample by the use of SThM devices. One of the first quantitative measurements carried out using the SThM equipment allowed determination of the thermal conductivity of diamond-like nanocomposite films [17]. The resistive ThP was made of a bent end etched Wollaston wire. The measurement was carried out in the constant temperature mode. The determination of the thermal conductivity was based on a comparison of powers required for holding the temperature of the ThP constant when it was in air and when it touched the sample. The thermal conductivity of the sample was read from the earlier determined calibration curve. In 1999 a new technique, based on the 3ω method [18], was proposed [19]. The Wollaston wire resistive ThP was heated by the AC current at a frequency ω, and the 3ω component of the voltage drop on the probe was recorded as a function of the frequency. The analysis of experimental data was based on the theoretical model of the "classical" 3ω method. The thermal conductivity was determined from the dependence of the 3ω signal amplitude on the frequency. In 2005 Lefévre and Volz [20], considering the thermal model of the Wollaston wire resistive ThP, showed that experimental data obtained in such SThM experiments in the AC mode are difficult to be interpreted based on the theory of the 3ω method. They found that the thermal conductivity of the sample mainly influences the amplitude of the 3ω signal at low frequencies and that this amplitude remains constant over a certain frequency range. So, to determine the thermal conductivity of the sample, this amplitude must be measured.

The problem of modeling of the thermal measurement, which uses the resistive SThM probes made of Wollaston wire, was considered in many studies. The obtained results were summarized in a book chapter [21]. It was shown that information about the thermal conductivity of the sample can be retrieved from either DC or AC measurements carried out at a relatively low frequency. In the case of AC measurements, this information is contained mainly in the amplitude of the signal. The AC measurement is justified by a higher signal-to-noise ratio which can be achieved in lock-in detection. The detection at the 3rd harmonic allows rejection of signal components which do not contain information about the thermal conductivity of the sample. The spatial resolution of the measurement depends on the radius of the tip–sample contact, and it does not depend on the frequency.

The analysis of the development of quantitative measurements using SThM equipment presented above allows one to state that a well established thermal model of experiment using Wollaston wire ThP exists. Based on this model, methods for measurement of the thermal conductivity with submicron resolution were proposed [20,21]. However, other ThP probes for SThM are also available on the market (http://www.parkafm.com/New_html/resources/download.php?code=tutorial\&filename=SThM.pdf, http://veeco.com/mailing_list.aspx?File=%2fpdfs%2fdatabase_pdfs%2fVITA_Final.pdf). There are so-called nanofabricated thermal probes, which can be used to achieve better spatial resolution in both topographic and thermal measurements. However, according to the authors' knowledge, investigations in which nanofabricated probes had been used in the active mode to determine the thermal conductivity were not reported. Moreover, neither analytical nor numerical thermal models of these probes were proposed to analyze possibilities of application of nanofabricated probes for measurement of the local thermal conductivity. It is even difficult to find a detailed description of the geometry of these probes. All these facts

motivated us to develop a thermal model of the nanofabricated probe by the use of finite element analysis (FEA). According to this model, the influence of the thermal conductivity of the investigated sample on the temperature distribution in the probe was analyzed, and the applicability of the nanofabricated probe to the measurement of the thermal conductivity was considered. The possible additional thermal resistance between the probe and the sample caused by non-perfect thermal contact was also taken into account.

2 Geometry of the Probe

As was mentioned in Sect. 1, the detailed specification of nanofabricated thermal probes used in XE-series AFM is hardly available. These probes are fabricated using micromachining, low pressure chemical vapor deposition, and electron beam lithography [22]. The substrate for the probe fabrication is a 500 nm thick Si_3N_4 plate. One end of the plate has a triangular shape with a tip angled away from the substrate plane at 56°. The apex of the angled part is about 12 μm over the substrate plane. The resistive film (NiCr and Pt) and the gold contact pads are deposited on this substrate. Photographs of the probe are shown in Fig. 1. Basic information about such probes sold by PSIA Inc. as Nano Thermal Probes (NThP) can be found in http://www.parkafm.com/New_html/resources/download.php?code=tutorial\&filename=SThM.pdf. The electrical resistance of NThP is in the range of 200 Ω to 650 Ω, and their thermal coeffi-

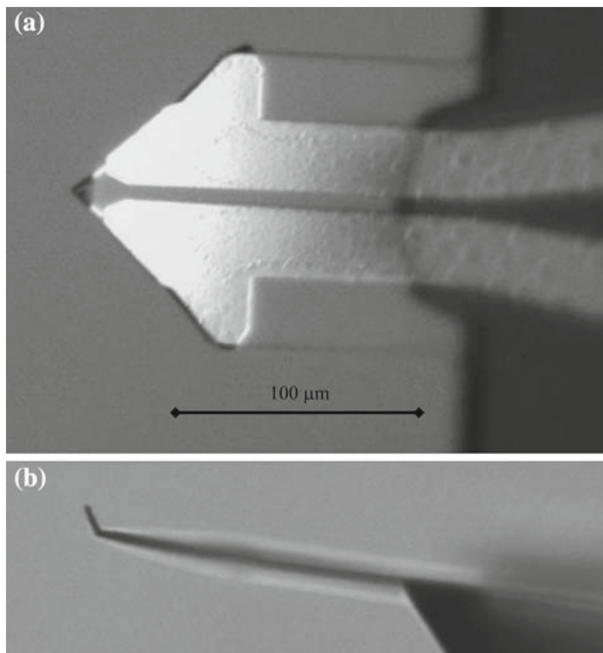

Fig. 1 (**a**) Bottom and (**b**) Side views of the Thermal Nano Probe from PSIA Inc

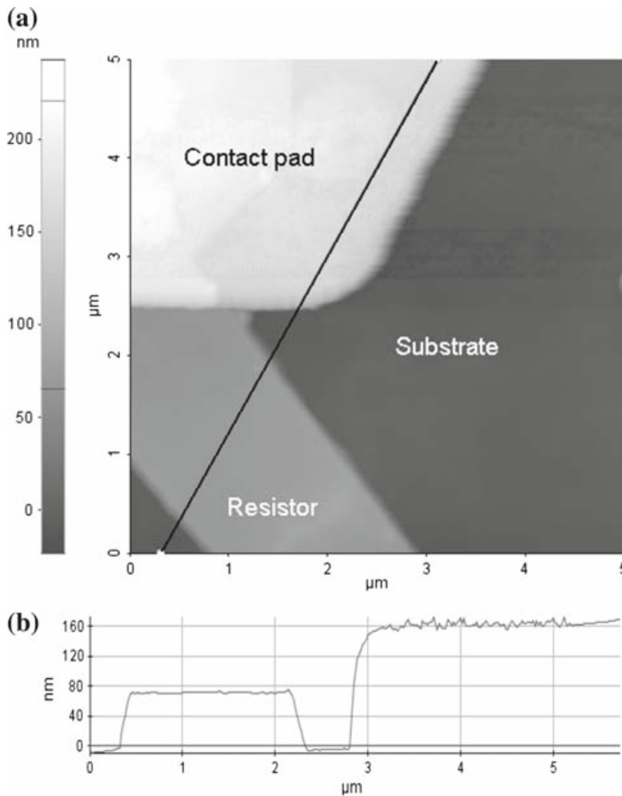

Fig. 2 (**a**) Topography of the selected region of NThP with visible resistor and contact pad and (**b**) Surface profile along marked *straight line*

cient of resistance is $1.23 \times 10^{-3}\text{K}^{-1}$. The tip radius is 100 nm. The current through the probe should not exceed 1 mA.

For correct modeling of the heat transport in the probe, thicknesses of metal films deposited on Si_3N_4 substrate must be known. An AFM image of the selected region of the NThP surface is shown in Fig. 2a. The deposited resistive layer and gold contact pad are clearly visible. As follows from the profile shown in Fig. 2b, the resistor is about 70 nm thick and the thickness of the gold contact pad is about 160 nm. The image of the end of the probe obtained by scanning electron microscopy (SEM) (Fig. 3) reveals that the resistive layer becomes narrower near the apex of the probe. The resistor width decreases from 2 µm near the contact pad to less than 1 µm near the apex. In accordance with AFM and SEM images, a geometrical model of the NThP was created. The small flat surface at the apex assures well-defined contact to the sample.

For modeling heat transport in the NThP, the probe geometry was simplified. Only the triangular end of the probe was left, and the tip was straightened out. Because the considered structure has a symmetry plane, it is sufficient to analyze the heat transport in half of the probe. The sample was modeled by a relatively big cuboid touching the small flat area at the apex. The described geometry is shown schematically in Fig. 4.

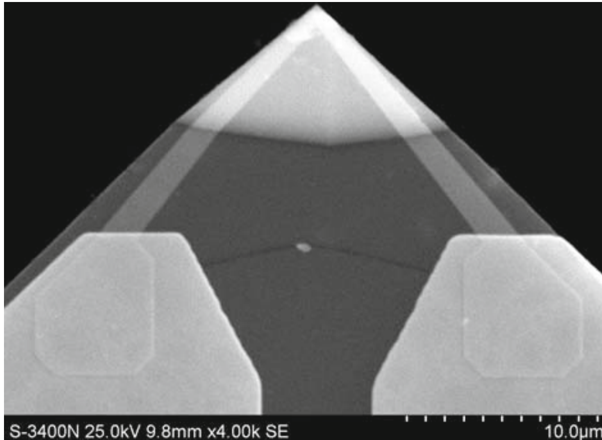

Fig. 3 Scanning electron microscopy image of the ending of the NThP. The deposited resistive film and gold contact pads are clearly visible

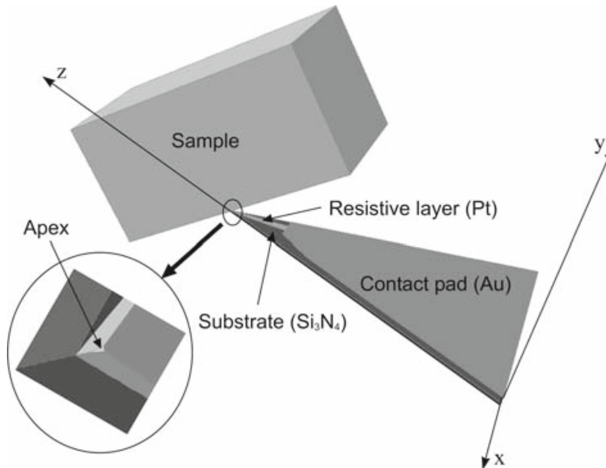

Fig. 4 Geometrical model of the NThP probe and the sample used for analysis of the influence of the thermal conductivity of the sample on the temperature distribution in the probe

3 Modeling of the Heat Transport in the Probe–Sample System

The goal of this work is to analyze possibilities of quantitative measurement of the thermal conductivity by the use of NThP. Such measurement will be possible if changes in the thermal conductivity of the sample influence the temperature distribution in the resistive film. The analysis requires a thermal model of the probe. The geometry of the probe, even after some simplifications described in the last paragraph of the previous section, is quite complicated. Therefore, it is quite difficult to propose an analytical model of the heat transport in the NThP. This is the reason for modeling the heat transport numerically by finite element analysis (FEA). The model was built

Table 1 Thermal conductivities of materials used in the model

Model element	Material	Thermal conductivity (293 K) ($W \cdot m^{-1} \cdot K^{-1}$)
Substrate	Si_3N_4	33
Resistive layer	Pt	72
Contact pad	Au	317
Sample	Different materials (i.e., diamond, Si, Fe, Cu, V, glass, etc.)	0.17–2320

using COMSOL Multiphysics software. After determining the geometry, the thermal parameters of all elements and boundary conditions at all surfaces and interfaces were defined. The basic properties of materials used in the model are collected in Table 1.

Three kinds of boundary conditions were used in the model. The plane $x = 0$ is the symmetry plane of the system, so for all surfaces belonging to this plane, ideal thermal insulation was assumed (heat flux through this plane is equal to zero). The assumption that the temperature and heat flux are continuous at all inner boundaries was made. Heat sources in the system are localized close to the probe apex, so it is reasonable to assume that far from the apex the probe is at ambient temperature. The same conditions exist for the sample. So, the surfaces of the sample except the symmetry plane and the surface touched by the probe apex, and the surface of the probe at $z = 0$ were at ambient temperature. Convective heat exchange to the air at the remaining outer surfaces was assumed.

For this analysis the boundary between the probe apex and the sample is of great importance. Its area is of the order of 10^{-14} m^2. Because the thermal contact between the probe apex and the sample may not be perfect, it was assumed that the heat flux through this contact is

$$j_Q = \frac{1}{R_{\mathrm{th}}} \left(T_{\mathrm{p}} - T_{\mathrm{s}}\right), \tag{2}$$

where R_{th} is the thermal resistance of the contact, and T_{p} and T_{s} are temperatures of the apex and the sample surface contacting the apex, respectively. For the ideal contact, $R_{\mathrm{th}} = 0$ and the condition of the continuity of the temperature and the heat flux is obtained.

The next step of the development of the thermal model of the NThP is the determination of heat sources in the system. It was assumed that heat sources arise only as a result of electric current flow through the resistive layer. Because this layer becomes narrower in the direction of the apex, the volume density of heat sources also grows in this direction. The resistive layer width, d, can be considered as a linear function of the z coordinate;

$$d = d_0 - \gamma z, \tag{3}$$

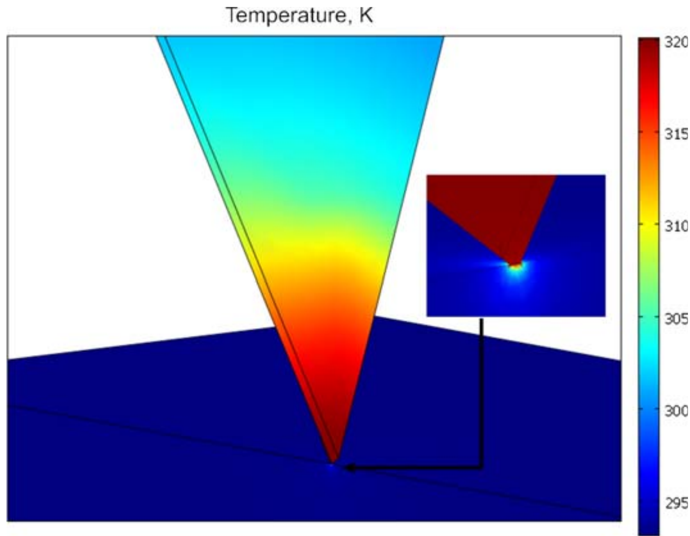

Fig. 5 Image of the temperature distribution in the probe and the sample near the probe–sample contact. The sample material was titanium

where d_0 and γ are constants. A straightforward analysis leads to the conclusion that the volume density of the heat source in the resistive layer can be written as

$$w = \frac{A}{(d_0 - \gamma z)^2}, \tag{4}$$

where A is a parameter depending on the thickness and electrical resistivity of the resistive layer and the electrical current through it.

The described model can be used to calculate numerically the temperature distribution in the probe–sample system shown in Fig. 4. Exemplary results of such calculations, obtained for titanium as the sample ($\kappa = 7.5\,\mathrm{W \cdot m^{-1} \cdot K^{-1}}$), are presented in Fig. 5. The heat sources in the resistive layer cause a rise in temperature near the sharp end of the probe. The heat flux through the probe apex to the sample perturbs the temperature distribution. The analysis of the dimensions of the disturbed region in the sample leads to the conclusion that the disturbance penetrates into the sample at a distance comparable to the linear dimension of the apex. Consequently, the spatial resolution of thermal measurements using NThP is defined by the dimensions of the probe apex. Possibilities of application of NThP to quantitative thermal measurements are analyzed in the next section.

4 Use of NThP for Quantitative Measurements: Numerical Analysis

As was mentioned in the previous section, the aim of this investigation is to analyze possibilities of applications of NThP to the measurement of the local thermal conductivity of the sample. The signal recorded by the SThM is related to changes in

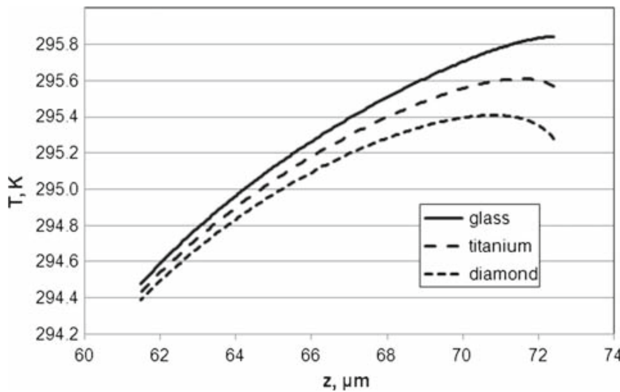

Fig. 6 Temperature distributions along the resistive layer determined for glass ($\kappa = 1.1\,\mathrm{W \cdot m^{-1} \cdot K^{-1}}$), titanium ($\kappa = 21.9\,\mathrm{W \cdot m^{-1} \cdot K^{-1}}$), and diamond ($\kappa = 2320\,\mathrm{W \cdot m^{-1} \cdot K^{-1}}$) samples; the ambient temperature $T_a = 293\,\mathrm{K}$

the electrical resistance of the resistive layer. The thermal model of the probe can be used to define the temperature distribution along the resistive layer. Such distributions obtained for three samples with different thermal conductivities are shown in Fig. 6. The influence of the thermal conductivity of the sample on the temperature distribution in the resistive layer is evident. Since the coefficient of thermal resistance of this layer is known, the relative change in the probe resistance caused by the temperature rise can be calculated as an integral or a sum along z. If the temperature rises $\Delta T(z_i)$ relatively to the ambient temperature in N equidistance points along the resistive layer are determined, the relative change in the probe resistance is

$$\delta R = \frac{\Delta R}{R_0} = \chi_R \sum_{i=1}^{N} \frac{\Delta T(z_i)}{d_0 - \gamma z_i} \Bigg/ \sum_{i=1}^{N} \frac{1}{d_0 - \gamma z_i}, \tag{5}$$

where χ_R is the coefficient of thermal resistance (equal to $1.23 \times 10^{-3}\,\mathrm{K^{-1}}$ for NThP). In the presented model, $d_0 = 10\,\mu\mathrm{m}$, $\gamma = 0.128$, and z_i changes from 61.5 µm to 72.4 µm. The dependence of the relative changes in the electrical resistance of the probe on the thermal conductivity of the sample is shown in Fig. 7. The calculations were carried out for the same distribution of heat sources in the resistive layer. Over the whole considered range of the thermal conductivity, an increase in the thermal conductivity of the sample causes a decrease in the probe resistance. The best sensitivity of the probe resistance to the thermal conductivity changes is observed between $2\,\mathrm{W \cdot m^{-1} \cdot K^{-1}}$ and $200\,\mathrm{W \cdot m^{-1} \cdot K^{-1}}$.

In the considered thermal model of the probe, two mechanisms of heat abstraction from the heated region were assumed: the convection to the surrounding gas (air) and the conduction to the sample and to the probe holder. The second mechanism should depend on the thermal conductivity of the probe substrate. Therefore, it seems to be interesting to examine the influence of the substrate thermal conductivity on the

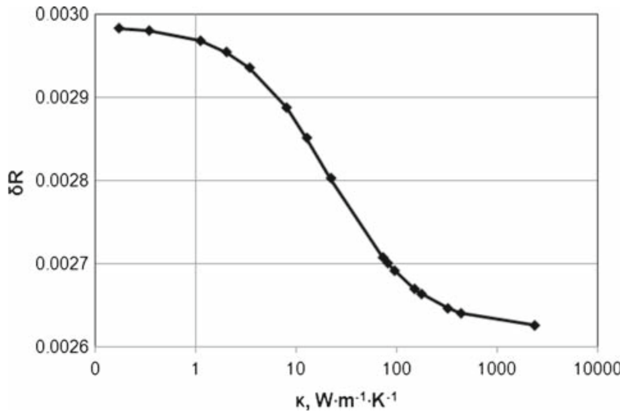

Fig. 7 Relative changes in the electrical resistance ($\delta R = \frac{\Delta R}{R_0}$) of NThP caused by temperature rise in the resistive layer as a function of the thermal conductivity of the sample. Calculations were done for the same distribution of heat sources in the resistive layer and different samples

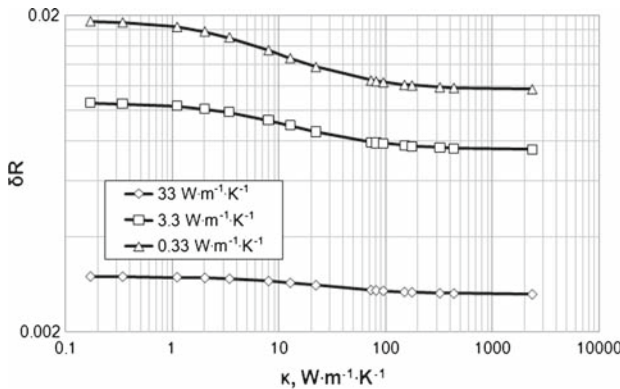

Fig. 8 Relative changes in the electrical resistance ($\delta R = \frac{\Delta R}{R_0}$) of NThP as a function of the thermal conductivity of the sample. Calculations were done for different thermal conductivities of the probe substrate

sensitivity of the probe to the thermal conductivity of the sample. Results presented in Fig. 8 show that the sensitivity of the probe to the sample thermal conductivity increases with decreases in the thermal conductivity of the probe substrate. Generally, the lower is the thermal conductivity of the probe substrate, the higher are the relative resistance changes caused by probe heating. More detailed analysis of Fig. 8 reveals also a shift of the region of maximum sensitivity toward lower thermal conductivities along with decreases of the thermal conductivity of the probe substrate.

The next problem which should be considered is the influence of the quality of the probe–sample contact on the dependence of the resistance changes on the thermal conductivity of the sample. It was assumed that an additional thermal resistance can exist between the probe apex and the sample. In the thermal model, this resistance was simulated by a 20 nm thick film between the probe apex and the sample.

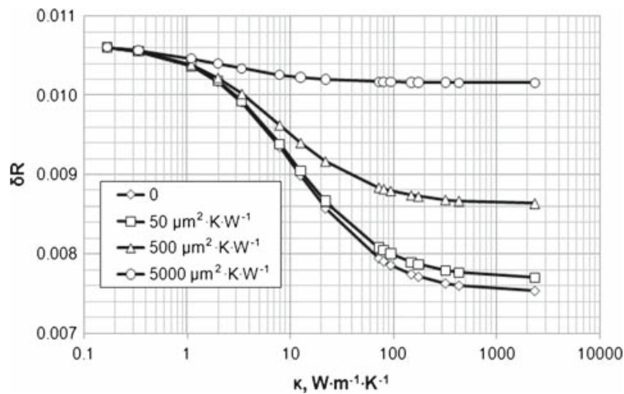

Fig. 9 Relative changes in the electrical resistance ($\delta R = \frac{\Delta R}{R_0}$) of NThP as a function of the thermal conductivity of the sample. Calculations were done for different additional thermal resistances at the probe–sample contact

Calculations were carried out for three different values of the thermal conductivity of this contact film: $4\,\mathrm{W \cdot m^{-1} \cdot K^{-1}}$, $40\,\mathrm{W \cdot m^{-1} \cdot K^{-1}}$, and $400\,\mathrm{W \cdot m^{-1} \cdot K^{-1}}$. These thermal conductivities correspond to the following thermal resistances of the contact: $5 \times 10^{-9}\,\mathrm{m^2 \cdot K \cdot W^{-1}}$, $5 \times 10^{-10}\,\mathrm{m^2 \cdot K \cdot W^{-1}}$, and $5 \times 10^{-11}\mathrm{m^2 \cdot K \cdot W^{-1}}$, respectively. In Fig. 9 dependences of the relative changes in the probe electrical resistance on the sample thermal conductivity obtained for different thermal resistances of the probe–sample contact are shown. The thermal resistance of the probe substrate was assumed to be $3.3\,\mathrm{W \cdot m^{-1} \cdot K^{-1}}$ in this case. The increase of the contact thermal resistance of the probe–sample contact causes a decrease of the dynamic range of changes in the probe electrical resistance. In real measurement it can lead to serious underestimation of the thermal conductivity of the sample. This problem is especially important in the investigation of good thermal conductors.

5 Preliminary Experimental Results

To verify correctness of dependences obtained from the FEA of the NThP, preliminary experiments were carried out. The measurements were done using XE-70 AFM (PSIA Inc.) equipped with a thermal module and data access module. It can be used to control the probe current with an external voltage and to register the signal with an external voltmeter. Similar to other experiments, the unbalanced voltage from the Wheatstone bridge with the probe in one arm was measured. The resistance NThP was used (904M-Kelvin from PSIA Inc.). The probe current was modulated at relatively low frequencies from 9 Hz to 25 Hz, and the amplitude of the unbalanced voltage at the 3rd harmonic was measured with a lock-in voltmeter (SR7265 from Signal Recovery). Since the amplitude practically did not depend on the modulation frequency, it was assumed that this amplitude was proportional to the change in the electrical resistance of the NThP in the DC mode. Measurements were carried out for three flat samples: glass, silicon, and single crystal 4H-SiC. The thermal conductivities of these

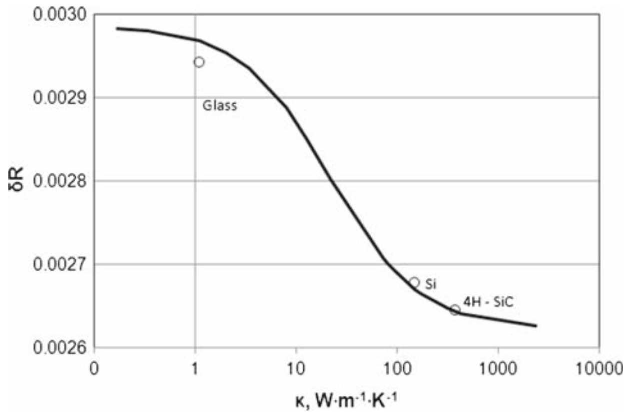

Fig. 10 Experimentally determined relative changes in the electrical resistance ($\delta R = \frac{\Delta R}{R_0}$) of the NThP probe. Experiment was carried out for glass ($\kappa = 1.1\ \mathrm{W \cdot m^{-1} \cdot K^{-1}}$), silicon ($\kappa = 148\ \mathrm{W \cdot m^{-1} \cdot K^{-1}}$), and 4H–SiC ($\kappa = 370\ \mathrm{W \cdot m^{-1} \cdot K^{-1}}$). The theoretical dependence is also shown (same as in Fig. 7)

materials are $1.1\ \mathrm{W \cdot m^{-1} \cdot K^{-1}}$, $148\ \mathrm{W \cdot m^{-1} \cdot K^{-1}}$, and $370\ \mathrm{W \cdot m^{-1} \cdot K^{-1}}$, respectively. The determined amplitudes were scaled by a constant factor and compared with the theoretical dependence of the relative changes in the electrical resistance of the NThP on the sample thermal conductivity. The results are shown in Fig. 10. The comparison has a qualitative character, but agreement between the numerically calculated curve and experimental points is satisfactory. Similar data for Wollaston probes can be found, e.g., see [21,23,24].

6 Conclusions

A batch nanofabricated ThP have become more and more popular in scanning thermal microscopy. They can be used to obtain better spatial resolution than Wollaston wire ThP and seem to have more reproducible parameters. However, the lack of a thermal model of NThP means that these ThP are not used for quantitative measurements of the local thermal conductivity. The thermal model of NThP proposed in this work was based on a finite element analysis method and can be used to analyze the temperature field in the probe–sample system. Furthermore, the relative change in the electrical resistance of the probe caused by the rise of the probe temperature can be calculated. The majority of currently available NThP includes resistive probes in which the information about the sample is deduced from changes of the electrical resistance of the probe.

The analysis showed that NThP can be used to measure the local thermal conductivity over a wide range of values. For the probe modeled in this work the best sensitivity to the changes of the sample thermal conductivity was obtained in the range of $2\ \mathrm{W \cdot m^{-1} \cdot K^{-1}}$ to $200\ \mathrm{W \cdot m^{-1} \cdot K^{-1}}$. From a practical point of view, it is important that the probe sensitivity strongly depends on the thermal conductivity of the probe substrate. The lower is the thermal conductivity of the substrate, the bigger is the

sensitivity to the changes in the sample thermal conductivity. However, for the case of probes fabricated on the substrate with low thermal conductivity, the maximum sensitivity range shifts toward lower thermal conductivities.

The fundamental significance for proper interpretation of the measured data obtained by the use of NThP has the quality of the thermal contact between the probe apex and the sample. The additional thermal resistance at this contact can lead to considerable underestimation of the thermal conductivity of the sample, especially for samples of high thermal conductivity.

Because basic parameters of nanofabricated thermal probes are scattered, e.g., their thermal resistance can change from 200 Ω to 650 Ω, each NThP should be calibrated before quantitative measurement using a few reference samples with very different thermal conductivities.

The presented analysis should be treated as a simplified one. Such effects as the dependence of the thermal conductivity on temperature, radiative losses, etc. were not taken into account. Nevertheless, the main conclusions concerning the usefulness of NThP for quantitative thermal measurements seem to be justified. Also, the agreement between the numerical analysis and experimental results is satisfactory.

References

1. D.G. Cahill, K. Goodson, A. Majumdar, J. Heat Transf. **124**, 223 (2002)
2. P.K. Schelling, L. Shi, K.E. Goodson, Mater. Today **8**, 30 (2005)
3. X. Hu, A.A. Padilla, J. Xu, T.A. Fisher, K.E. Goodson, ASME J. Heat Transf. **128**, 1109 (2006)
4. J.P. Reifenberg, M.A. Panzer, S. Kim, A.M. Gibby, Y. Zhang, S. Wong, H.S. Wong, K.E. Goodson, Appl. Phys. Lett. **91**, 111904 (2007)
5. T.W. Kenny, K.E. Goodson, J.G. Santiago, E.N. Wang, J.M. Koo, L. Jiang, E. Pop, S. Sinha, L. Zhang, D. Fogg, S. Yao, R. Flynn, C.H. Cheng, C.H. Hidrovo, Int. J. High Speed Electron. Syst. **16**, 107 (2006)
6. J. Bodzenta, Ann. Chim. Sci. Mat. **32**, 401 (2007)
7. T. Luo, J. Lloyd, J. Heat Transf. **130**, 122403 (2008)
8. K.-M. Liu, W. Chen, L.F. Register, S.K. Banerjee, J. Appl. Phys. **104**, 114515 (2008)
9. B. Krenzer, A. Hanisch, A. Duvenbeck, B. Rethfeld, M. Horn-von Hoegen, J. Nanomater. **2008**, 590609 (2008)
10. J.A. Rowlette, K.E. Goodson, IEEE Trans. Electron. Dev. **55**, 220 (2008)
11. C.C. Williams, H.K. Wickramasinghe, Appl. Phys. Lett. **49**, 1587 (1986)
12. G. Binning, C.F. Quate, Ch. Gerber, Phys. Rev. Lett. **56**, 930 (1986)
13. C.C. Williams, H.K. Wickramasinghe, Proc. IEEE Ultrason. Symp. (1986)
14. A. Majumdar, Ann. Rev. Mater. Sci. **29**, 505 (1999)
15. H.M. Pollock, A. Hammiche, J. Phys. D **34**, R23 (2001)
16. B. Cretin, S. Gomés, N. Trannoy, P. Vairac, Topics Appl. Phys. **107**, 181 (2007)
17. F. Ruiz, W.D. Sun, F.H. Pollak, Ch. Venkatraman, Appl. Phys. Lett. **73**, 1802 (1998)
18. D.G. Cahill, Rev. Sci. Instrum. **61**, 802 (1990)
19. G. Fiege, A. Altes, R. Heiderhoof, L. Balk, J. Phys. D **32**, L13 (1999)
20. S. Lefévre, S. Volz, Rev. Sci. Instrum. **76**, 033701 (2005)
21. M. Chirtoc, J.-S. Antoniow, J.-F. Henry, P. Dole, J. Pelzl, in , ed. by J.L. Bubendorff, F.H. Lei Advanced Techniques and Applications on Scanning Probe Microscopy (Transworld Research Network, Kerala, 2008), p. 197
22. G. Mills, H. Zhou, A. Midha, L. Donaldson, J.M.R. Weaver, Appl. Phys. Lett. **72**, 2900 (1998)
23. L. Thiery, E. Gavignet, B. Cretin, Rev. Sci. Instrum. **80**, 034901 (2009)
24. M. Chirtoc, J. Gibkes, R. Wernhardt, J. Pelzl, A. Wieck, Rev. Sci. Instrum. **79**, 093703 (2008)